Renormalized dipole moment operator in the second half of the $2p$-$1f$ shell

B. Ghosh and S. K. Sharma
Department of Physics, Indian Institute of Technology Kanpur, Kanpur-208016, India
(Received 24 May 1983)

Renormalized single-particle matrix elements of the magnetic dipole moment operator for the $(2p_{3/2}, 1f_{5/2}, 2p_{1/2})$ space are calculated in the framework of perturbation theory involving first- and second-order excitations from the $1f_{7/2}$ core. The calculated dipole matrix elements are consistent with the empirical values deduced from the observed $M1$ transitions as well as dipole moments in several Ni and Cu isotopes.

NUCLEAR STRUCTURE Renormalized magnetic dipole moment operator; restricted valence space spanned by the $2p_{3/2}$, $1f_{5/2}$, and $2p_{1/2}$ orbits; first- and second-order diagrams; empirical values of the effective $M1$ single-particle matrix elements.

I. INTRODUCTION

The mass region $A=57-70$ has been extensively studied[1] both theoretically and experimentally in recent years. A number of explicit shell-model calculations[2-6] have revealed that the energy spectra of low-lying-states in the Ni and Cu isotopes can be fairly well described in the $(2p_{3/2}, 1f_{5/2}, 2p_{1/2})$ space provided reasonable effective two-body interactions are employed between the active nucleons outside the ^{56}Ni core. However, the omission of the $1f_{7/2}$ orbit from the configuration space necessitates the use of effective electromagnetic operators for a successful explanation of various transition rates as well as static moments. In this connection, Glaudemans[7] and Koops[8] have recently found that the effect of the polarization of the $1f_{7/2}$ core cannot be described simply in terms of a renormalization of the g factors. They have, therefore, obtained the effective $M1$ single particle matrix elements by treating them as free parameters in a least-squares fit to the recent experimental data involving 13 $M1$ transitions in $^{57-61}$Ni, 14 $M1$ transitions in $^{59-65}$Cu, and 11 dipole moments in $^{57-65}$Ni, $^{60-65}$Cu.

The purpose of this paper is to demonstrate that the empirical $M1$ single-particle matrix elements, which exhibit significant deviation from the Schmidt values, can be understood in a microscopic perspective in terms of the contributions resulting from various first- and second-order diagrams describing the excitation processes from the $1f_{7/2}$ core.

In Sec. II we present an explicit evaluation of the contributions resulting from first- as well as second-order graphs. The results of our calculation are given and discussed in Sec. III. Our main conclusions are presented in Sec. IV.

II. EXPRESSIONS FOR FIRST- AND SECOND-ORDER DIAGRAMS

The perturbed state $|\psi\rangle$ in terms of the unperturbed state $|\phi_{jm}\rangle$ is given by[9-11]

$$|\psi\rangle = |\phi_{jm}\rangle + \frac{P}{\epsilon_j - H_0} V |\phi_{jm}\rangle + \cdots , \tag{2.1}$$

where we have taken zeroth-order energy in the denominator, thereby limiting ourselves to only the connected diagrams in the theory.[11]

The perturbation series for the effective matrix element of the μ operator is, therefore, given by

$$\begin{aligned}\frac{\langle\psi'|\mu^{(0)}|\psi\rangle}{(\langle\psi'|\psi'\rangle\langle\psi|\psi\rangle)^{1/2}} &= \langle\phi_{j'm}|\mu^{(0)}|\phi_{jm}\rangle + \langle\phi_{j'm}|\mu^{(0)}\frac{P}{\epsilon_j - H_0}V|\phi_{jm}\rangle + \langle\phi_{j'm}|V\frac{P}{\epsilon_{j'}-H_0}\mu^{(0)}|\phi_{jm}\rangle \\ &+ \langle\phi_{j'm}|\mu^{(0)}\frac{P}{\epsilon_j - H_0}V\frac{P}{\epsilon_j - H_0}V|\phi_{jm}\rangle + \langle\phi_{j'm}|V\frac{P}{\epsilon_{j'}-H_0}V\frac{P}{\epsilon_{j'}-H_0}\mu^{(0)}|\phi_{jm}\rangle \\ &+ \langle\phi_{j'm}|V\frac{P}{\epsilon_{j'}-H_0}\mu^{(0)}\frac{P}{\epsilon_j - H_0}V|\phi_{jm}\rangle \\ &- \tfrac{1}{2}\langle\phi_{j'm}|\mu^{(0)}|\phi_{jm}\rangle\left[\langle\phi_{jm}|V\frac{P}{\epsilon_j - H_0}\frac{P}{\epsilon_j - H_0}V|\phi_{jm}\rangle\right. \\ &\left. + \langle\phi_{j'm}|V\frac{P}{\epsilon_{j'}-H_0}\frac{P}{\epsilon_{j'}-H_0}V|\phi_{j'm}\rangle\right] + \cdots ,\end{aligned} \tag{2.2}$$

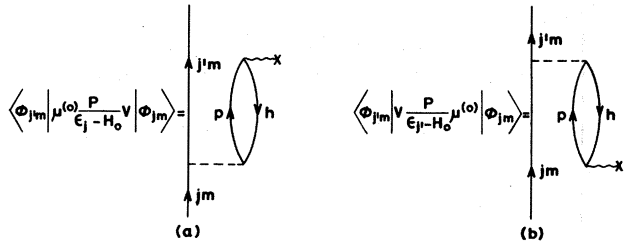

FIG. 1. First-order renormalization of magnetic dipole moment operator (exchange diagrams are implied).

where $\mu^{(0)}$ denotes a bare magnetic moment operator.

The diagrams corresponding to the first- and second-order terms are given in Figs. 1 and 2, respectively. Evaluating Fig. 1(a) yields the contribution

$$-\sum_{m_h,m_p}\frac{\langle j'm,pm_p\,|\,V\,|\,jm,hm_h\rangle\langle hm_h\,|\,\mu^{(0)}\,|\,pm_p\rangle}{\epsilon_j-\epsilon_{j'}+\epsilon_h-\epsilon_p}\,. \tag{2.3}$$

Here we have suppressed the isotopic spin labels. The two-body matrix element appearing in (2.3) can be expressed as

$$\langle j'm,pm_p\,|\,V\,|\,jm,hm_h\rangle = \sum_J (j'pmm_p\,|\,Jm+m_p)(jhmm_h\,|\,Jm+m_h)\times\langle j'p\,|\,V\,|\,jh\rangle_J\,. \tag{2.4}$$

The matrix element $\langle hm_h\,|\,\mu^{(0)}\,|\,pm_p\rangle$ can be factored as follows by using the Wigner-Eckart theorem:

$$\langle hm_h\,|\,\mu_z^{(0)}\,|\,pm_p\rangle=(1pOm_p\,|\,hm_h)\langle h[\mu^{(0)}p]^h\rangle\,. \tag{2.5}$$

The task of carrying out the summations over the magnetic projections is facilitated by the use of the formula (A1) given in Appendix A. Thus one obtains the contribution

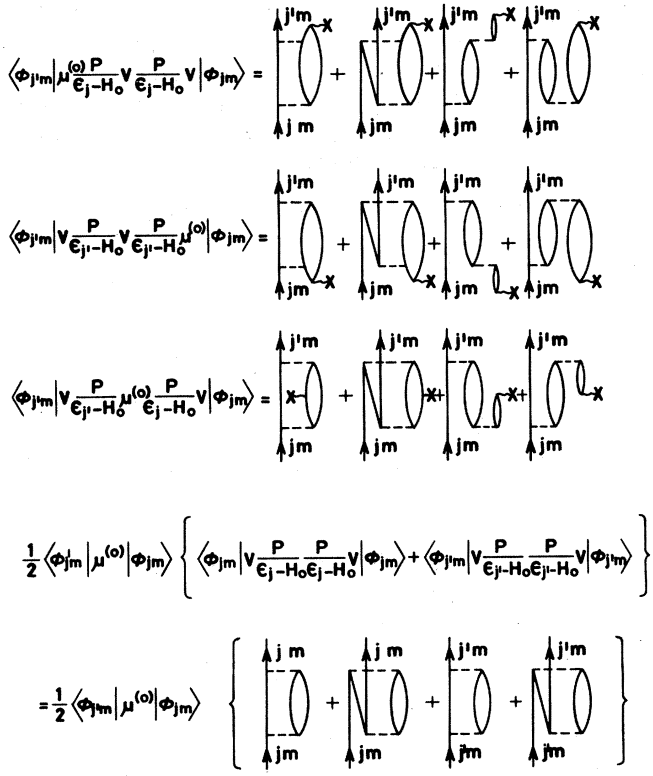

FIG. 2. Second-order terms contributing to the renormalization of magnetic dipole moment operator (exchange diagrams are implied).

$$\left[\sum_J(2J+1)\left[\frac{2j_p+1}{2j+1}\right]^{1/2}(-1)^{j'+j_p-J}(j'1-mO\,|\,j-m)\times\langle j'j_p\,|\,V\,|\,jj_h\rangle_J W(j'pjh,J1)\langle j_p[\mu^{(0)}j_h]^{j_p}\rangle\right]\frac{1}{\epsilon_j-\epsilon_{j'}+\epsilon_h-\epsilon_p}\,. \tag{2.6}$$

It is convenient to rewrite the magnetic moment operator

$$\mu^{(0)}=\sum_{i(p,n)}[g_1(i)\vec{1}(i)+g_s(i)\vec{s}(i)] \tag{2.7}$$

in terms of two operators μ_1 and μ_2 such that

$$\mu^{(0)}=\mu_1+\mu_2\tau_0^{(1)}\,, \tag{2.8}$$

where

$$\mu_1=0.5(g_1^p+g_1^n)\vec{1}+0.5(g_s^p+g_s^n)\vec{s},\quad \mu_2=0.5(g_1^p-g_1^n)\vec{1}+0.5(g_s^p-g_s^n)\vec{s}\,. \tag{2.9}$$

One may finally write the contribution of Fig. 1(a) in terms of the operators μ_1 and μ_2 as follows:

$$\left[\frac{2j_p+1}{2j+1}\right]^{1/2}(j'1-mO\,|\,j-m)\left[\frac{\langle j_p[\mu_1 j_h]^{j_p}\rangle\langle j_p j_h^{-1}\,|\,V\,|\,jj'^{-1}\rangle_{10}}{\epsilon_j-\epsilon_{j'}+\epsilon_h-\epsilon_p}+(-1)^{\tau_j-1/2}\frac{\langle j_p[\mu_2 j_h]^{j_p}\rangle\langle j_p j_h^{-1}\,|\,V\,|\,jj'^{-1}\rangle_{11}}{\epsilon_j-\epsilon_{j'}+\epsilon_h-\epsilon_p}\right]. \tag{2.10}$$

The contribution of Fig. 1(b) comes directly from (2.10) if we interchange j and j'.

We have given here the general expressions for the first-order renormalization of the $M1$ single-particle matrix elements; these expressions reduce to the ones derived earlier by Mavromatis and co-workers[9,10] in connection with the correction to magnetic dipole moments in some $2s$-$1d$ shell nuclei.

We now discuss an explicit evaluation of various second-order graphs. The contribution arising from Fig. 3(a) involving $2p$-$1h$ intermediate states is

$$\sum_{j_1m_1,j_2m_2,j_3m_3,j_4m_4} \langle j_1m_1,j_2m_2 \mid V \mid jm,j_4m_4\rangle\langle j_1m_1,j_3m_3 \mid V \mid j'm,j_4m_4\rangle \times \left[\frac{1}{\epsilon_j-\epsilon_{j_1}-\epsilon_{j_2}+\epsilon_{j_4}}\right]\left[\frac{1}{\epsilon_{j'}-\epsilon_{j_1}-\epsilon_{j_3}+\epsilon_{j_4}}\right](-1)\langle j_2m_2 \mid \mu^{(0)} \mid j_3m_3\rangle \,. \tag{2.11}$$

Here we have suppressed the isotopic spin levels for the various single-particle states involved. Carrying out the summation over the magnetic projections with the help of the identity (B2) given in Appendix B one obtains

$$\frac{-(1j'Om \mid jm)}{\sqrt{2j+1}} \sum_{\substack{j_1j_2\\ j_3j_4}} (-1)^{j_2+j_3}(2j_2+1)^{1/2}\left[\frac{1}{(\epsilon_j-\epsilon_{j_1}-\epsilon_{j_2}+\epsilon_{j_4})(\epsilon_{j'}-\epsilon_{j_1}-\epsilon_{j_3}+\epsilon_{j_4})}\right] \times \sum_{\substack{J_1J_2\\ T_1T_2}} (2J_1+1)(2J_2+1)W(1J_2jj_4;J_1j')W(1j_3J_1j_1;j_2J_2)\langle j_1j_2 \mid V \mid j'j_4\rangle_{J_1T_1}\langle j_1j_3 \mid V \mid jj_4\rangle_{J_2T_2}(2T_1+1) \times[\langle j_2[\mu_1j_3]^{j_2}\rangle\delta_{T_1T_2}+(-1)^{\tau_j-1/2}\langle j_2[\mu_2j_3]^{j_2}\rangle(2T_2+1)W(1T_2\tfrac{1}{2}\tfrac{1}{2};T_1\tfrac{1}{2})W(1\tfrac{1}{2}T_1\tfrac{1}{2};\tfrac{1}{2}T_2)] \,. \tag{2.12}$$

Here μ_1 and μ_2 refer to the isoscalar and isovector part of the magnetic operator defined in (2.8).

The contribution corresponding to the five diagrams shown in Figs. 3(b)—(f) can easily be related to that of Fig. 3(a); the various diagrams shown in Fig. 3 differ from each other only in their energy denominators.

The contribution of the diagrams shown in Fig. 4 can be expressed in a similar manner by the following expression

$$-\frac{(1-j'O-m \mid j-m)}{2\sqrt{2j+1}} \sum_{\substack{j_1j_2\\ j_3j_4}} (2j_3+1)^{1/2}\left[\frac{1}{(\epsilon_j-\epsilon_{j_1}-\epsilon_{j_2}+\epsilon_{j_3})(\epsilon_{j'}-\epsilon_{j_1}-\epsilon_{j_2}+\epsilon_{j_4})}-\frac{1}{(\epsilon_j-\epsilon_{j_1}-\epsilon_{j_2}+\epsilon_{j_3})(\epsilon_j-\epsilon_{j'}+\epsilon_{j_3}-\epsilon_{j_4})}\right. -\frac{1}{(\epsilon_{j'}-\epsilon_j+\epsilon_{j_3}-\epsilon_{j_4})(\epsilon_{j'}-\epsilon_{j_1}-\epsilon_{j_2}+\epsilon_{j_3})}+\frac{1}{(\epsilon_{j_1}-\epsilon_{j'}+\epsilon_{j_2}-\epsilon_{j_4})(\epsilon_{j_1}-\epsilon_j+\epsilon_{j_2}-\epsilon_{j_3})} \left.-\frac{1}{(\epsilon_{j_1}-\epsilon_{j'}-\epsilon_{j_2}+\epsilon_{j_4})(\epsilon_j-\epsilon_{j'}-\epsilon_{j_3}+\epsilon_{j_4})}-\frac{1}{(\epsilon_{j'}-\epsilon_j+\epsilon_{j_3}-\epsilon_{j_4})(\epsilon_{j_1}-\epsilon_j+\epsilon_{j_2}-\epsilon_{j_4})}\right] \times \sum_{JT}(2J+1)W(1j_4jJ;j_3j')\langle j_1j_2 \mid V \mid j'j_4\rangle_{JT}\langle j_1j_2 \mid V \mid jj_3\rangle_{JT}(2T+1) \times\left[\frac{\langle j_3[\mu_1j_4]^{j_3}\rangle}{2}+(-1)^{\tau_j+1/2}W(1\tfrac{1}{2}\tfrac{1}{2}T;\tfrac{1}{2}\tfrac{1}{2})\langle j_3[\mu_2j_4]^{j_3}\rangle\right] . \tag{2.13}$$

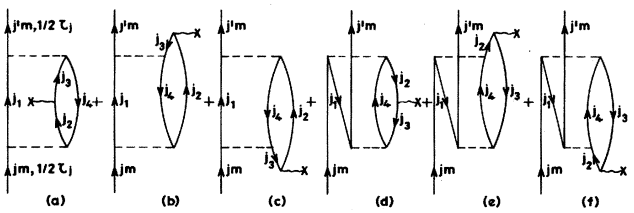

FIG. 3. Diagrams involving $2p$-$1h$ [(a)—(c)] and $3p$-$2h$ [(d)—(f)] intermediate states. The magnetic moment operator operates on a particle intermediate state in (a) and on a hole intermediate state in (d) (exchange diagrams are implied).

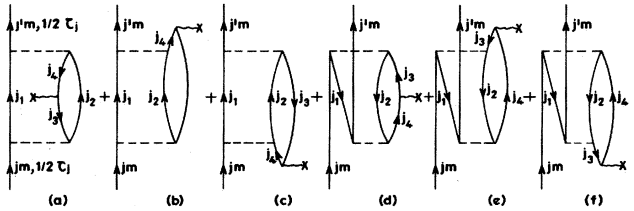

FIG. 4. Diagrams involving $2p$-$1h$ [(a)—(c)] and $3p$-$2h$ [(d)—(f)] intermediate states. The magnetic moment operator operates on a hole intermediate state in (a) and on a particle intermediate state in (d) (exchange diagrams are implied).

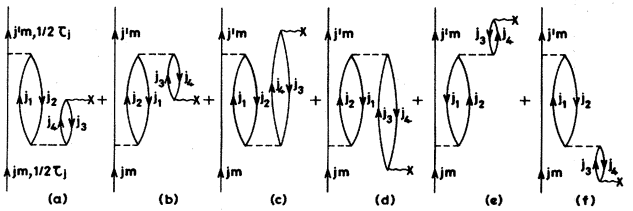

FIG. 5. Second-order TDA [(a)—(d)] and RPA [(e) and (f)] diagrams (exchange diagrams are implied).

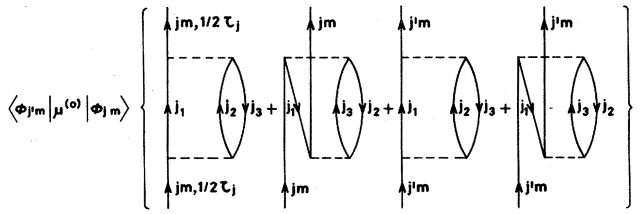

FIG. 6. Second-order core renormalization diagrams (exchange diagrams are implied).

The Tamm-Dancoff (TDA) and random-phase approximations (RPA) diagrams of Fig. 5 give

$$\frac{(1j'Om\,|\,jm)}{\sqrt{2j+1}}\sum_{\substack{j_1j_2\\ j_3j_4}}(2j_4+1)^{1/2}\left[\frac{1}{(\epsilon_{j_2}-\epsilon_{j_1}+\epsilon_{j_3}-\epsilon_{j_4})(\epsilon_{j'}-\epsilon_j-\epsilon_{j_1}+\epsilon_{j_2})}\right.$$

$$+\frac{1}{(\epsilon_j-\epsilon_{j'}+\epsilon_{j_1}-\epsilon_{j_2})(\epsilon_{j_1}-\epsilon_{j_2}-\epsilon_{j_3}+\epsilon_{j_4})}+\frac{1}{\epsilon_{j_2}-\epsilon_{j_1}+\epsilon_{j_3}-\epsilon_{j_4})(\epsilon_j-\epsilon_{j'}+\epsilon_{j_3}-\epsilon_{j_4})}$$

$$+\frac{1}{(\epsilon_{j'}-\epsilon_j-\epsilon_{j_3}+\epsilon_{j_4})(\epsilon_{j_1}-\epsilon_{j_2}-\epsilon_{j_3}+\epsilon_{j_4})}+\frac{1}{(\epsilon_j-\epsilon_{j'}+\epsilon_{j_1}-\epsilon_{j_2})(\epsilon_j-\epsilon_{j'}+\epsilon_{j_3}-\epsilon_{j_4})}$$

$$\left.+\frac{1}{(\epsilon_{j'}-\epsilon_j-\epsilon_{j_3}+\epsilon_{j_4})(\epsilon_{j'}-\epsilon_j-\epsilon_{j_1}+\epsilon_{j_2})}\right]$$

$$\times\left[\sum_{\substack{J_1J_2\\ T_1T_2}}\langle jj_1\,|\,V\,|\,j'j_2\rangle_{J_1T_1}(2J_1+1)W(1j_2jJ_1;j_1j')\right.$$

$$\times\langle j_2j_3\,|\,V\,|\,j_1j_4\rangle_{J_2T_2}(2J_2+1)W(1j_3j_1J_2;j_4j_2)$$

$$\left.\times(2T_1+1)(2T_2+1)\left[\frac{\langle j_4[\mu_1j_3]^{j_4}\rangle}{4}-(-1)^{1/2+\tau_j}W(1\tfrac{1}{2}\tfrac{1}{2}T_1;\tfrac{1}{2}\tfrac{1}{2})\right.\right.$$

$$\left.\left.\times\,W(1\tfrac{1}{2}\tfrac{1}{2}T_2;\tfrac{1}{2}\tfrac{1}{2})\langle j_4[\mu_2j_3]^{j_4}\rangle\right]\right]. \tag{2.14}$$

Finally, the contribution of the core renormalization diagrams shown in Fig. 6 is given by the expression

$$-\frac{\langle j'm\,|\,\mu^{(0)}\,|\,jm\rangle}{8(2j+1)}\sum_{j_1j_2j_3}\sum_{JT}(2J+1)(2T+1)\left[\frac{|\langle j_1j_2\,|\,V\,|\,jj_3\rangle_{JT}|^2}{(\epsilon_j-\epsilon_{j_1}-\epsilon_{j_2}+\epsilon_{j_3})^2}+\frac{|\langle j_1j_2\,|\,V\,|\,j'j_3\rangle_{JT}|^2}{(\epsilon_{j'}-\epsilon_{j_1}-\epsilon_{j_2}+\epsilon_{j_3})^2}\right]. \tag{2.15}$$

III. RESULTS AND DISCUSSIONS

We have employed here as an effective interaction a modified version of the Kuo-Brown (KB) interaction[12] which had earlier[13] explained successfully the observed suppression of $M1$ as well as $M3$ moments in ^{57}Ni. The lowest-energy Hartree-Fock (HF) solution obtained with this version of the KB interaction (labeled in Ref. 13 as the KB2 interaction) is found to be spherical with the structure $(1f_{7/2})^{16}_{J=0}$. As pointed out earlier,[13] the unmodified KB interaction does not satisfy the observed deformation systematics in the $2p$-$1f$ shell; in particular, it does not reproduce the $1f_{7/2}$ subshell closure. The minimum-energy HF solution resulting from the KB interaction is, in fact, deformed.

The spherical, minimum-energy solution for ^{56}Ni resulting from the KB2 interaction is characterized by a gap of about 6.8 MeV. The spherical single-particle energies re-

TABLE I. First- and second-order renormalization of the single-particle dipole moment operator (in units of μ_N) for valence neutrons. Here the notation $\langle j_1 \| \mu \| j_2 \rangle$ stands for the matrix element $\langle j_1 \frac{1}{2} \| \mu \| j_2 \frac{1}{2} \rangle$. The empirical values obtained by Koops (Ref. 8) from a chi-square fit to the data in Ni and Cu isotopes involving the MSDI and the ASDI effective interactions for the ($2p_{3/2}$-$2p_{1/2}$-$1f_{5/2}$) space are given. The values obtained by Glaudemans and others (Refs. 5 and 7) resulting from a fit to the data on only Ni isotopes are also given. In the MSDI and ASDI cases, the matrix element $\langle \frac{1}{2} \| \mu \| \frac{1}{2} \rangle$ could not be determined by the available data.

			$\langle j_1 \| \mu^{(1)} \| j_2 \rangle_\nu$		$\langle j_1 \| \mu^{(2)} \| j_2 \rangle_\nu$				Empirical values[a]		
j_1	j_2	$\langle j_1 \| \mu^{(0)} \| j_2 \rangle_\nu$	Proton	Neutron	Figs. 3 and 4	Fig. 5	Fig. 6	$\langle j_1 \| \mu^{(0)}+\mu^{(1)}+\mu^{(2)} \| j_2 \rangle_\nu$	MSDI	ASDI	Refs. 5 and 7
$\frac{1}{2}$	$\frac{1}{2}$	0.64	−0.25	−0.10	−0.01	0.20	−0.05	0.43			1.13
$\frac{1}{2}$	$\frac{3}{2}$	1.80	−0.39	−0.92	0.01	0.90	−0.24	1.16[b]	0.49(8)	0.34(7)	0.80
$\frac{3}{2}$	$\frac{3}{2}$	−0.64	0.11	0.26	0.09	−0.23	0.12	−0.29	−0.30(2)	−0.29(2)	−0.30
$\frac{3}{2}$	$\frac{5}{2}$	0.00	−0.19	0.29	0.05	−0.11	0.00	0.04[c]	0.27(5)	0.27(4)	0.27
$\frac{5}{2}$	$\frac{5}{2}$	0.27	−0.08	−0.10	0.01	0.11	−0.05	0.16	0.10(1)	0.10(1)	0.10

[a]These values are taken from Ref. 8. The numbers in the parentheses give the errors resulting from the fit multiplied with the square root of χ^2. In the case of Refs. 5 and 7, the average absolute deviation between theory and experiment for the available $M1$ transitions, ranging between 0.01 and 0.14 W.u., is 0.03 W.u.

[b]The calculated value of the transposed matrix element is 1.20. The correction due to non-Hermiticity inherent in the truncated perturbation series [Eq. (2.2)] is thus quite small.

[c]The calculated value of the transposed matrix element is −0.13.

sulting from this spherical solution are employed as the unperturbed energies for the orbits $2p_{3/2}$, $2p_{1/2}$, and $1f_{5/2}$.

The results of our first-order perturbative calculations are presented in columns 4 and 5 of Tables I and II. It is seen that the first-order calculation can account for a large part of the discrepancy between the Schmidt values and the empirical ones. A comparison of the results presented in column 4 of Table I with those given in column 5 of Table II reveals that the contribution of the core protons towards the first-order renormalization of the neutron single-particle matrix elements is comparable in magnitude to the contribution of the core neutrons towards a renormalization of the proton matrix elements. This can be understood in terms of the involvement of the same channel of interaction—the neutron-proton channel—in both cases. The contributions, however, are of opposite signs mostly because of the differences between the proton and the neutron g_s factors. In a similar manner one can explain as to why the contribution (column 5 of Table I) of the core neutrons towards a renormalization of the neutron single-particle matrix elements is almost the same in magnitude (but of opposite sign) as the contribution (column 4 of Table II) of the core protons towards the proton matrix elements.

van Hees *et al.*[6] have recently examined the effect of explicit inclusion of the $1f_{7/2}$ hole on the Schmidt values in ^{57}Ni; their shell model calculation involved the KB interaction in conjunction with an empirical value of the $1f_{7/2}$-$2p_{3/2}$ separation which is smaller by only about 0.5 MeV compared to the spherical HF value employed here. It is interesting to note that the shell model results involving $1p\,1h$ states are comparable to our first-order perturbative estimates.

Next we discuss the second-order contributions to the Schmidt values of various matrix elements. The contributions arising from various second-order diagrams

TABLE II. First- and second-order renormalization of the single-particle dipole moment operator for valence protons. As mentioned in Ref. 8, the matrix elements $\langle \frac{1}{2} \| \mu \| \frac{1}{2} \rangle$ and $\langle \frac{5}{2} \| \mu \| \frac{5}{2} \rangle$ could not be determined through a chi-square fit to the available data.

			$\langle j_1 \| \mu^{(1)} \| j_2 \rangle_\pi$		$\langle j_1 \| \mu^{(2)} \| j_2 \rangle_\pi$				Empirical values[a]	
j_1	j_2	$\langle j_1 \| \mu^{(0)} \| j_2 \rangle_\pi$	Proton	Neutron	Figs. 3 and 4	Fig. 5	Fig. 6	$\langle j_1 \| \mu^{(0)}+\mu^{(1)}+\mu^{(2)} \| j_2 \rangle_\pi$	MSDI	ASDI
$\frac{1}{2}$	$\frac{1}{2}$	−0.26	0.12	0.21	−0.07	−0.20	0.02	−0.18		
$\frac{1}{2}$	$\frac{3}{2}$	−2.16	1.11	0.33	0.06	−0.92	0.29	−1.29[b]	−0.99(16)	−0.68(17)
$\frac{3}{2}$	$\frac{3}{2}$	1.26	−0.31	−0.09	0.05	0.23	−0.24	0.90	0.88(4)	0.86(4)
$\frac{3}{2}$	$\frac{5}{2}$	0.00	−0.34	0.16	0.02	0.12	0.00	−0.04[c]	−0.75(12)	−0.44(14)
$\frac{5}{2}$	$\frac{5}{2}$	0.17	0.12	0.07	0.02	−0.11	−0.03	0.24		

[a]Reference 8.

[b]The calculated value of the transposed matrix element is −1.35.

[c]The calculated value of the transposed matrix element is −0.11.

displayed in Fig. 2 have been presented in columns 6–8 of Tables I and II. The contributions resulting from the TDA and RPA graphs (Fig. 5) as well as those due to the core renormalization graphs (Fig. 6) have been given separately. It may be mentioned here that the intermediate states involved in our second-order calculation correspond to excitations from the occupied ($1f_{7/2}$ shell) orbital to the unoccupied $2p$-$1f$ shell orbitals, with the energy denominators ranging from about 13.2 to 19.3 MeV. The KB interaction employed here has already been partially renormalized by ^{40}Ca core excitation processes; these processes cannot be described within the $2p$-$1f$ shell space. The use of the unrenormalized KB interaction would clearly necessitate an explicit involvement of higher-order intermediate states.

From the results presented in columns 6–8 one notices that the overall second-order corrections are not very large. This is seen to be mainly due to a partial cancellation of the contribution resulting from the TDA (or RPA) graphs and the renormalization graphs. One also finds that the sum of the contributions resulting from the diagrams given in Figs. 3 and 4 is consistently quite small. This is related to the fact that these diagrams have an energy denominator (expression 2.12)

$$\frac{1}{(\epsilon_j-\epsilon_{j_1}-\epsilon_{j_2}+\epsilon_{j_4})(\epsilon_{j'}-\epsilon_{j_1}-\epsilon_{j_3}+\epsilon_{j_4})}\approx\left[\frac{1}{2\Delta E_{ph}}\right]^2 .$$

The diagrams shown in Fig. 5, on the other hand, possess energy denominators which are approximately $(1/\Delta E_{ph})^2$.

It is interesting to compare the present results with those obtained earlier[10] by Mavromatis and Zamick in the case of the dipole moments of the ground states of the nuclei ^{29}Si and ^{209}Bi; they had obtained comparatively large dequenching, arising from the TDA and RPA graphs, together with small contributions from the renormalization term. Ripka and Zamick[14] later found that the large dequenching is associated with the existence of deformed HF minimum in ^{29}Si. The absence of large dequenching in the present work can, therefore, be related with the fact that the minimum-energy HF solution for ^{56}Ni is spherical; the deformed HF solution occurs at an excitation energy of about 6.8 MeV.

In columns 9–12 (Tables I and II) we have compared the renormalized values of the $M1$ matrix elements with their empirical values obtained by Koops.[8] We find that the renormalized values for the diagonal matrix elements $\langle \frac{3}{2} \| \mu \| \frac{3}{2} \rangle_\nu$, $\langle \frac{5}{2} \| \mu \| \frac{5}{2} \rangle_\nu$, and $\langle \frac{3}{2} \| \mu \| \frac{3}{2} \rangle_\pi$ are in excellent agreement with the empirical values obtained by Koops as well as by Glaudemans. It may be mentioned that the empirical value of the $\langle \frac{3}{2} \| \mu \| \frac{3}{2} \rangle_\nu$ matrix element is just the observed magnetic moment in ^{57}Ni. In the case of the matrix element $\langle \frac{1}{2} \| \mu \| \frac{3}{2} \rangle_\nu$, whereas the renormalized value agrees reasonably with the fitted value obtained by Glaudemans, it shows a discrepancy of about 0.67 μ_N and 0.82 μ_N, respectively, with the empirical values obtained by Koops in conjunction with the modified surface-delta interaction (MSDI) and the adjusted surface-delta interaction (ASDI). The renormalized matrix element $\langle \frac{1}{2} \| \mu \| \frac{3}{2} \rangle_\pi$ is in acceptable agreement with the fitted value resulting from the MSDI interaction. However the empirical value for this matrix element resulting from the ASDI interaction shows a discrepancy of 0.61 μ_N. Further, our results for the renormalization of the matrix elements $\langle \frac{3}{2} \| \mu \| \frac{5}{2} \rangle_{\nu,\pi}$ indicate that it is difficult to account for the fitted values of these matrix elements in terms of the present perturbative framework involving only the $2p$-$1f$ shell orbits; the large empirical values may be imitating the effects of intruder states arising from excitation of the ^{40}Ca core as well as of higher-order diagrams within the $2p$-$1f$ shell.

In view of the fact that the present perturbative calculation yields unambiguous estimates for the renormalization of the diagonal matrix elements $\langle j \| \mu \| j \rangle_{\pi,\nu}$—the off-diagonal ones are not determined uniquely due to the non-Hermiticity inherent in Eq. (2.2)—we have also expressed their renormalized values in terms of the effective g factors which define the generalized $M1$ operator

$$\vec{\mu}=g_l'\,\vec{l}+g_s'\,\vec{s}+g_p(Y^{(2)}s^{(1)})^{(1)} .$$

Whereas we obtain the values $g_l^{\pi'}=0.93$, $g_s^{\pi'}=3.44$, and $g_p^{\pi}=1.71$ in the case of the renormalization of the magnetic moment operator for the valence proton, we obtain the values $g_l^{\nu'}=0.03$, $g_s^{\nu'}=-1.72$, and $g_p^{\nu}=-0.90$ in the case of the valence neutron. The renormalized values of the $\langle j \| \mu \| j \rangle_{\pi,\nu}$ matrix elements thus imply a significant reduction in the spin g factor as well as a sizable contribution from the spin-polarization term $(Y^{(2)}s^{(1)})^{(1)}$.

IV. CONCLUSIONS

We have calculated here the one-body matrix elements of the effective dipole moment operator in the $(2p_{3/2},2p_{1/2},1f_{5/2})$ space by taking into account the renormalization effects due to excitations from the closed $1f_{7/2}$ core. It turns out that the empirical values of the $M1$ matrix elements can be explained reasonably well in most of the cases in a microscopic, parameter-free manner in terms of the contributions resulting from various first- and second-order graphs.

A major motivation in undertaking this work was a desire to examine the validity of a perturbative approach in the context of the renormalization of electromagnetic operators in the second half of the $2p$-$1f$ shell. We have seen that a calculation involving just the first- and second-order graphs is successful because of the large energy denominators involved. Enomoto *et al.*[15] have sometime ago reported a strong suppression of the $M3$ part of magnetic scattering in nuclei involving a closed $f_{7/2}$ shell. The present work suggests that it may be possible to understand the observed anomalous momentum transfer dependence in $M3(q)$ in terms of first- and second-order core-excitation processes.

We wish to thank Dr. J. E. Koops for communicating some of his results prior to publication.

APPENDIX A

Using the identity

$$(af\alpha\gamma-\alpha\,|\,c\gamma)U(abcd;ef)=\sum_{\beta}(ab\alpha\beta\,|\,e\alpha+\beta)(ed\alpha+\beta\gamma-\alpha-\beta\,|\,c\gamma)(bd\beta\gamma-\alpha-\beta\,|\,f\gamma-\alpha) \tag{A1}$$

we obtained

$$\begin{aligned}\sum_{m_p m_h}&\langle j'm,j_pm_p\,|\,V\,|\,jm,j_hm_h\rangle\langle j_pm_p\,|\,\mu^{(0)}\,|\,j_hm_h\rangle\delta_{m_pm_h}\\&=\sum_J\sum_{m_p}(j'j_pmm_p\,|\,Jm+m_p)(jj_hmm_h\,|\,Jm+m_h)(1j_hOm_h\,|\,j_pm_p)\langle j_p[\mu^{(0)}j_h]^{j_p}\rangle\langle j'j_p\,|\,V\,|\,jj_h\rangle_J\\&=\sum_J(2J+1)\left[\frac{2j_p+1}{2j+1}\right]^{1/2}(-1)^{j'+j_p-J}(j'1-mO\,|\,j-m)W(j'pjh;J1)\langle j_p[\mu^{(0)}j_h]^{j_p}\rangle\langle j'j_p\,|\,V\,|\,jj_h\rangle_J\,.\end{aligned} \tag{A2}$$

APPENDIX B

We have

$$\begin{aligned}(ak\alpha\epsilon-\alpha\,|\,h\epsilon)U(afhg;ck)U(abcd;ef)=\sum_{\beta\delta}&(ab\alpha\beta\,|\,e\alpha+\beta)(ed\alpha+\beta\gamma-\alpha-\beta\,|\,c\gamma)(bd\beta\delta-\beta\,|\,f\delta)\\&\times(cg\alpha+\delta\epsilon-\alpha-\delta\,|\,h\epsilon)(fg\delta\epsilon-\alpha-\delta\,|\,k\epsilon-\alpha)\,.\end{aligned} \tag{B1}$$

Using this we obtained

$$\begin{aligned}\sum_{m_1m_2m_3m_4}&(1j_3Om_3\,|\,j_2m_2)(j_1j_2m_1m_2\,|\,J_1m_1+m_2)(j_1j_3m_1m_3\,|\,J_2m_1+m_3)\\&\times(jj_4mm_4\,|\,J_1m+m_4)(j'j_4mm_4\,|\,J_2m+m_4)\\&=\frac{-(1j'Om\,|\,jm)}{\sqrt{2j+1}}(-1)^{j_2+j_3}(2j_2+1)^{1/2}(2J_1+1)(2J_2+1)W(1J_2jj_4;J_1j')W(1j_3J_1j_1;j_2J_2)\,.\end{aligned} \tag{B2}$$

[1] J. E. Koops and P. W. M. Glaudemans, Z. Phys. A 280, 181 (1977), and the references contained therein.

[2] E. A. Phillips and A. D. Jackson, Phys. Rev. 169, 917 (1968).

[3] S. S. M. Wong, Nucl. Phys. A159, 235 (1970).

[4] P. W. M. Glaudemans, M. J. A. De Voigt, and E. F. M. Steffens, Nucl. Phys. A198, 609 (1972).

[5] M. C. Wang, H. C. Chang, H. T. Hsieh, and E. K. Lin, Nuovo Cimento A 29, 49 (1975).

[6] A. G. M. van Hees, P. W. M. Glaudemans, and B. C. Metsch, Z. Phys. A 293, 327 (1979).

[7] P. W. M. Glaudemans, in *Proceedings of the Sixth European Physical Society Nuclear Divisional Conference on the Structure of Medium-Heavy Nuclei, Rhodes, Greece, 1979,* edited by the "Demokritos" Tandem Accelerator Group, Athens (The Institute of Physics, Bristol, London, 1979), p. 11.

[8] J. E. Koops, thesis, Utrecht University, 1978.

[9] H. A. Mavromatis, L. Zamick, and G. E. Brown, Nucl. Phys. 80, 545 (1966).

[10] H. A. Mavromatis and L. Zamick, Nucl. Phys. A104, 17 (1967).

[11] P. J. Brussaard and P. W. M. Glaudemans, *Shell-Model Applications in Nuclear Spectroscopy* (North-Holland, Amsterdam, 1977).

[12] T. T. S. Kuo and G. E. Brown, Nucl. Phys. A114, 241 (1968).

[13] S. K. Sharma, Phys. Lett. 62B, 259 (1976); 102B, 85 (1981).

[14] G. Ripka and L. Zamick, Phys. Lett. 23B, 347 (1966).

[15] A. Enomoto, in *Proceedings of the Conference on Electron and Photo-excitation, Sendai, Japan, 1977,* edited by Y. Kawazoe (Laboratory of Nuclear Science, Tohoku University, Sendai, Japan, 1977), p. 173.